

## Imaging UXO Using Electrical Impedance Tomography

William Daily<sup>1</sup>, Abelardo Ramirez<sup>1</sup>, Robin Newmark<sup>1</sup>  
and Victor George<sup>2</sup>

<sup>1</sup>Lawrence Livermore National Laboratory, Livermore, Calif. 94550

<sup>2</sup>Roy F. Weston, Vallejo, Calif. 94592

### ABSTRACT

This paper reports the results of tests where electrical impedance tomography (EIT) was evaluated as a tool for detecting and locating buried unexploded ordnance (UXO). The method relies on the electrolytic polarization induced at the boundary between soil and buried metal. This induced polarization (IP) produces a measurable phase delay between the electric current imposed on the subsurface and the resulting voltage distribution. If natural sources of induced polarization are small compared to those due to buried metal objects, then tomographs of impedance phase may be used to indicate where metal-soil polarization may be present.

Three controlled tests were performed at a field site containing inert UXO buried in known locations. These tests produced a phase anomaly of about 20 milliradians that closely matched the known location of buried UXO objects. A fourth uncontrolled or blind test was performed under a building without prior knowledge of UXO presence. That test yielded phase anomalies as high as 75 milliradians. Limited excavation was performed at some of these anomalies but only a small amount (a few tens of grams) of metal was recovered. More extensive excavations are too costly until the building is razed.

### BACKGROUND

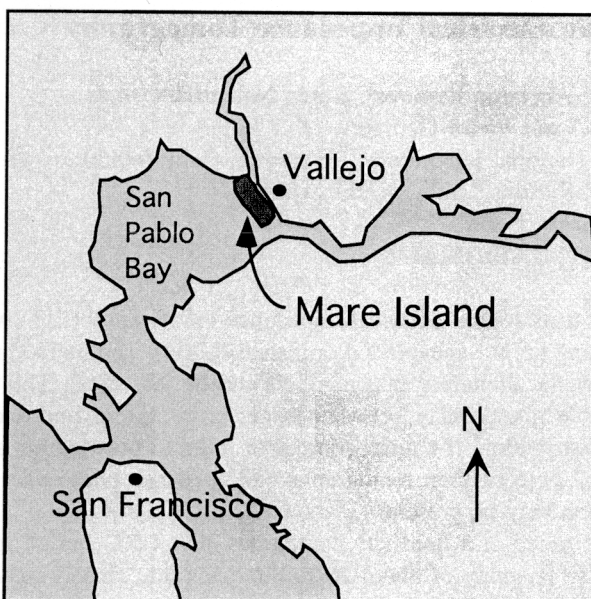
Locating UXO is a partially solved problem, meaning that many solutions exist but none work universally. UXO is typically detected using magnetometers, metal detectors, ground penetrating radar or controlled source electromagnetic induction. Except for the radar, these techniques provide little information regarding the depth of burial of potential targets and are sensitive to cultural artifacts such as metal fences, power lines or buildings. Factors that affect performance of traditional methods include soil moisture content, depth of burial or non-metallic targets. In some cases, the soil itself generates signals that can confuse the diagnostic method and data interpretation.

In this work, we evaluate another technology, electrical impedance tomography (EIT, also referred to as complex resistivity tomography or induced polarization tomography; Oldenberg and Li, 1994; Weller *et al.*, 1996; Shi *et al.*, 1998; Ramirez *et al.*, 1999), for locating buried UXO. EIT produces a tomograph or image of the subsurface electrical properties which can provide information regarding the target size, shape and depth. This information can be useful not only for detecting and locating the target but also for planning and monitoring remediation. The electrodes required to make EIT measurements can be deployed beneath and around buildings or other structures, so that surveys can be performed to sense under a building. Most other detection methods are blinded by interference from

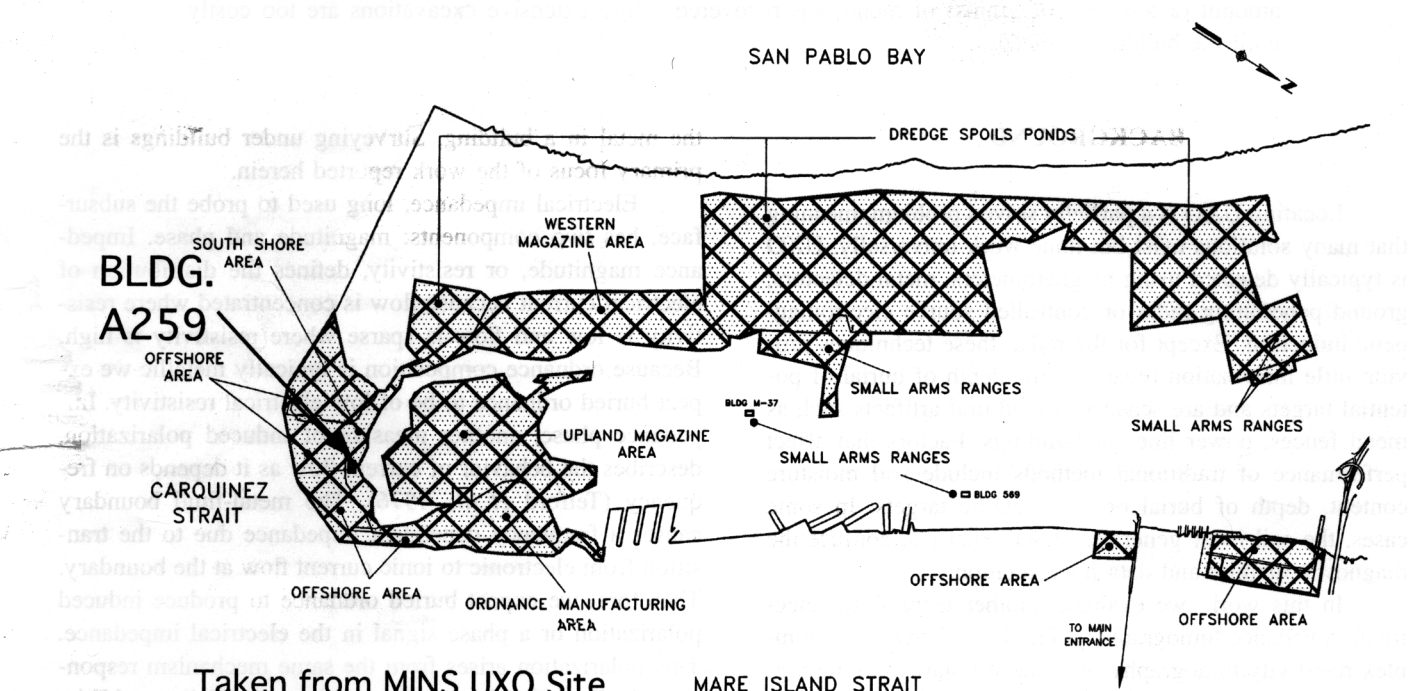
the metal in a building. Surveying under buildings is the primary focus of the work reported herein.

Electrical impedance, long used to probe the subsurface, has two components: magnitude and phase. Impedance magnitude, or resistivity, defines the distribution of electrical current because flow is concentrated where resistivity is low and flow is sparse where resistivity is high. Because ordnance composition is typically metallic we expect buried ordnance to be of low electrical resistivity. Impedance phase, another measure of induced polarization, describes the behavior of current flow as it depends on frequency (Telford *et al.*, 1976). The metal-fluid boundary causes a frequency dependant impedance due to the transition from electronic to ionic current flow at the boundary. Therefore, we expect buried ordnance to produce induced polarization or a phase signal in the electrical impedance. This polarization arises from the same mechanism responsible for the effect in metallic ore deposits (Keller and Frischknecht, 1966).

Mare Island, located near Vallejo, California, was a naval base beginning at the Civil War era and its mission included the manufacture, stockpiling and distribution of naval ordnance (Fig. 1). The Department of the Navy closed the base in 1996 and plans to return it to civilian control. However, large amounts of buried UXO have been discovered on site, delaying this transfer. Although sometimes the material is found scattered, a large accumulation of UXO is shown in Fig. 2. As a result, the U.S. Navy has



N



Taken from MINS UXO Site Investigation (1997)

**Figure 1. Location of the former Mare Island Naval Shipyard. Numerous areas are currently under investigation for buried UXO (after SSPORTS, 1997).**

supported an active remediation program to render the site safe for civilian use. The primary method for locating UXO has been magnetic surveys using portable magnetometers (U.S. Army Report, 1997). The method is fast, economical and easy to

use. However, due to interference from ferromagnetic and ferrimagnetic metal, the magnetometer cannot be used near or under buildings. At Mare Island there are many buildings which may have been built over buried UXO, and many of these buildings must be removed. Worker safety could be

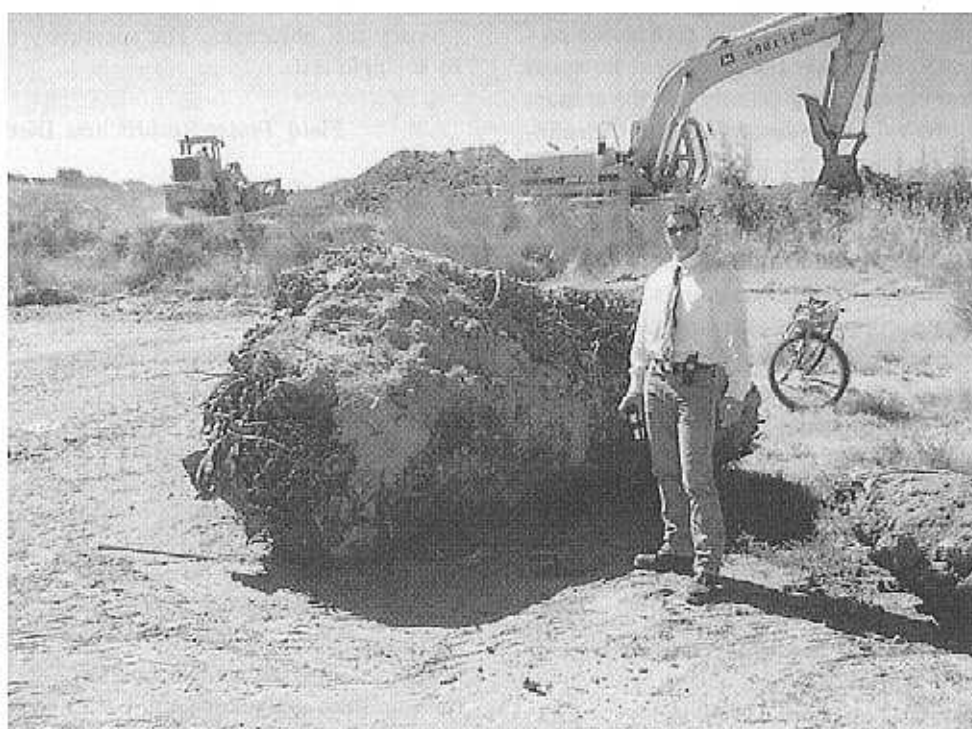


**Figure 2.** Buried mass excavated in dredge ponds at Mare Island. Contents of such masses include welding rods, silverware, china, tools, and a wide range of UXO.

improved if any UXO could be located and removed before a building is razed.

#### Electrical Impedance Tomography

Electrical impedance tomography (EIT) is a method that calculates subsurface images of electrical properties from a large number of impedance measurements. To image under a building, arrays of electrodes are placed beneath the structure where possible, or around the periphery where that is not possible. A low frequency (perhaps 0.125 to 1.0 Hz) current is driven between two electrodes. As this current flows through the ground under the building, it establishes voltages at the other electrodes that are measured and recorded. Two other electrodes are then used to drive current, and voltages are again measured on all other electrodes. This process is repeated until all linearly independent combinations of current and voltage measurements are made. For 30 electrodes, there are 405 such measurements ( $n(n - 3)/2$  where  $n$  is the number of electrodes).

The raw data are inverted to produce tomographic images of electrical properties in the ground. For the simpler case where the impedance is adequately described by the resistance only and the method is called electrical resistance tomography (ERT) (no phase difference between the current and voltage), the data processing has been described by Daily and Owen (1991), Oldenburg and Li

(1994), Sasaki (1992), and LaBrecque *et al.* (1996). Early adaptations of the technique to the field of geophysics were by Pelton *et al.* (1978), Dines and Lytle (1981), Tripp *et al.* (1984), Wexler *et al.* (1985). Adaptations for medical diagnostics can be found in Isaacson (1986), Barber and Seager (1987), and Yorkey *et al.* (1987).

Yang and LaBrecque (1999) describe a three-dimensional inversion algorithm which calculates impedance magnitude and phase tomographs; this algorithm is used for the work described herein. A two dimensional algorithm is also used in this work, as described in Ramirez *et al.* (1999). Other descriptions of EIT algorithms can be found in Oldenberg and Li (1994); Weller *et al.* (1996); Yuval and Oldenberg (1997); Shi *et al.* (1998). Here we only summarize the general structure of the algorithms used for this work. First, a numerical model of the subsurface electrical impedance is assumed, for which the voltage field is calculated. These calculated voltages are compared to those measured; they will be different because the computer model of the subsurface is only an initial guess. The model is then changed in such a way as to make the voltages calculated for the new model closer to those measured. The algorithm continues making changes to the numerical model, improving agreement between calculated and measured voltages. This iterative process is continued until the agreement is within some specified value that is related to the accuracy of the measured values.

Impedance magnitude (or electrical resistance) provides information about the resistance to current flow and is sensitive to such things as water salinity and the amount of water present in the soil. Impedance phase provides information about the electrical polarizability of the soil and is sensitive to metal (Van Voorhis *et al.*, 1973; Telford *et al.*, 1976) because the metal-ground water interface produces a phase delay between the transmitted current and the received voltage. Of course, the situation is more interesting than that because the phase also depends on pore fluid chemistry (Frye *et al.*, 1998; Keevil and Ward, 1962) and soil type (Marshall and Madden, 1959).

Some types of clay produce a small IP effect by membrane polarization but the polarization produced at a metal interface, called electrode polarization, is a different mechanism (Telford *et al.*, 1976). It is possible, therefore, that the two mechanisms will produce intrinsically different polarization that can be distinguished, perhaps by the spectral characteristics of the response. However, such discrimination is likely to be difficult and is beyond the scope of this project.

Of course, clay is ubiquitous in soils and so a small natural IP is common. How then can EIT be useful for detecting metal? First, an accumulation of buried metal may produce a polarization that is extrinsically different. For example, electrode polarization from metal is usually larger in magnitude than membrane polarization from clay—normally of small magnitude (less than about 10 mrad). In addition, UXO anomalies may be distinctively distributed (*e.g.*, lumped together, as expected from the fused masses typically found at Mare Island) instead of widely disseminated, like clay. For example, Fig. 2 is one of the larger masses found on the site, shown after excavation, and is a result of typical disposal practices: dig a hole, fill it up with UXO and other waste, cover to grade. With time the waste becomes loosely welded together as is evident in the figure. Therefore, UXO anomalies may be distinguishable since accumulations of clay like this mass are unlikely to occur naturally. Figure 2 represents one type of UXO target that might be found under buildings at Mare Island. We recognize, however, that the clay content of soils can vary greatly between sites and that the presence of clay may be a confusing influence in the EIT tests. Therefore, we chose a location for three controlled tests that would be as representative as possible of the natural IP at a fourth blind test site.

Our primary test objectives were to evaluate whether a buried accumulation or mass of UXO produces detectable IP signals and if that signal can be imaged reliably. After achieving these objectives, our secondary objective was to use the method in a blind test—on a site of unknown UXO content—and then excavate the site to determine the actual UXO content for comparison with a prediction based on EIT. Three different tests were performed to achieve the

primary test objectives. The secondary objective was met by a single test.

## Field Tests: Results and Discussion

### Controlled Tests—Site Description

We first describe three controlled tests related to our primary test objectives. Mare Island is located in Northern California within the San Francisco Bay region, where the Napa River enters San Pablo Bay (see Fig. 1). The former Mare Island Naval Shipyard complex occupies a peninsula extending into the San Pablo Bay. Rolling sandstone and shale hills at the southern end of Mare Island constitute the bedrock outcrops; the remainder of the land is predominantly flat low-lying fill areas and marshlands comprised of clay and silt. Parts of these low-lying areas are composed of naturally accreted sediments, accumulated after dikes were introduced along the southern portion of the island in the late 1800's. Dredge spoils and engineered fill material make up the remainder (SSPORTS, 1997). The controlled test site is only about 100 m from San Pablo Bay and is built up from dredge material out of the bay. The alluvium varies from fine silts to gravel with no recognizable structural units at the shallow depths of interest (top 3 m). The groundwater, only about 2 m from the surface, is brackish due to close proximity of the site to the bay. This site was chosen because it represented closely the soil conditions where the method might be used elsewhere at Mare Island.

The controlled test site was cleared of all UXO contamination that was detected using conventional means. An assortment of UXO (about 0.04 m<sup>3</sup>), taken from other locations at Mare Island, was then buried at this site in a single deposit at a depth between 0.5 and 1.0 m. Figure 3 shows the material before burial lying in the backhoe-excavated hole. Much of the material was brass, but iron and bronze components were included as well. Individual pieces ranged from fuses (about 1 cm diameter and 10 cm long) to cannon shells (about 20 cm diameter and over 30 cm long). All of the UXO material was in the same condition as originally exhumed, except for being rendered explosively inert. After the soil in the hole was compacted, the site was left undisturbed for about 3 weeks before the EIT measurements began. Our intention was to duplicate on a small scale the type of UXO target shown in Fig. 2.

A two-dimensional array of copper-copper sulfate electrodes (which have a low polarization; see Keller and Frischknecht, 1966) was placed on the ground surface over the buried target. Using this array, four-electrode impedance measurements were made which included all linearly independent combinations.

### Controlled Test—1

In the first controlled test, 30 electrodes were arranged at the surface around the edge of a small rectangular



**Figure 3.** Mass of UXO buried at the test site. A backhoe was used to dig the pit about 1 m deep and compact the backfill.

pattern, as might be used in a scaled up version, around the periphery of a building. The array is 5.1 m long and 1.8 m wide with electrode separation of 0.46 m. Results are shown in Fig. 4.

The inversion algorithm is two dimensional (*i.e.*, impedance can vary in the two horizontal dimensions but is uniform in the vertical dimension). This approximation to the three dimensional nature of the subsurface and UXO target means that reconstructed values can only be approximate. However, relative values should be preserved so that high or low parameter values caused by the target will be imaged. There are two reconstruction pixels (each 0.23 m square) between adjacent electrodes (spaced 0.46 m). For this sampling configuration the effective depth of investigation (the depth below which sensitivity falls off rapidly) is a little less than one meter (about half of the image plane width).

The UXO produces a weak conductive anomaly of about 1 Ohm-m in the impedance magnitude tomograph.

However, because there are natural variations in the soil that produce other regions even more conductive, the impedance magnitude (resistivity) cannot be used here as a reliable diagnostic of UXO.

The UXO target also produces a 15 to 20 mrad negative phase anomaly. This anomaly is consistent with a lag in the voltage waveform relative to the current as would be expected for "electrode polarization" between metallic and ionic conduction (Van Voorhis *et al.*, 197; Keller and Frischknecht, 1966). More importantly, this phase anomaly is significantly larger than the reconstructed phase of the surrounding soil at this site and therefore may be the discriminatory diagnostic that we are seeking. However, as discussed later, this result does not necessarily hold at all sites.

#### Controlled Test—2

A second test site was prepared about 100 m from the first; this site allowed us to determine whether UXO

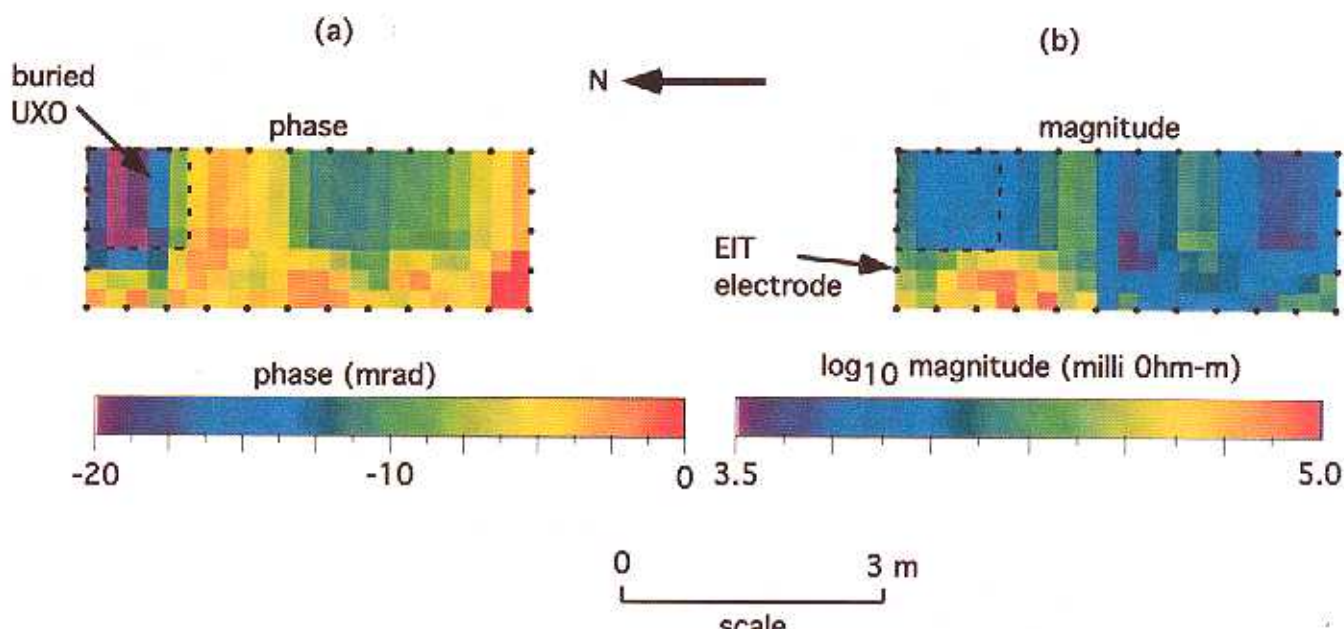


Figure 4. Two-dimensional impedance tomograph for controlled test 1 at Mare Island. Impedance phase (left tomograph) and impedance magnitude (right tomograph) with UXO buried under the area marked by the square outline. This 2D tomograph assumes constant values of impedance with depth. There are two pixels between adjacent electrodes and the measurement frequency is 0.5 Hz. (a) Phase in milliradians (mrad). (b) Resistivity in Ohm-m.

detectability was affected by variations in the local site conditions that are likely to be present at Mare Island. In this test, 30 electrodes were arranged on the surface with a 0.9 m spacing. The electrode array included electrodes on the perimeter of a 3.7 by 4.6 m rectangle as well as in its interior (as shown in Fig. 5). This electrode pattern might be used in buildings with significant crawl space where electrodes could be placed under the building (many of the buildings of interest at Mare Island sit on pilings raised about 1 meter above ground surface). The buried UXO target was the same in all essentials to that for the first controlled test.

The results of this test are shown in Fig. 5. The image format is different from that used on the previous site because the data were reconstructed using a fully three-dimensional inversion algorithm (described in Yang and LaBrecque, 1999). In contrast with Fig. 4, Fig. 5 shows a model in which the impedance varies both horizontally and vertically. This more general solution should yield a more faithful representation of the subsurface than the two-dimensional model used in the first test. Each reconstruction voxel is 0.3 m on a side and there are three voxels between adjacent electrodes. Unlike in Fig. 4, these 3D results are spatially smoothed so that individual mesh elements are not noticeable. In part (b) the phase reconstruction is rendered transparent between 0 and -13 mrad so that the anomaly can be seen in the 3D volume. The transparency threshold

for this, as well as the other images to be shown later, is somewhat arbitrary.

The impedance magnitude, or resistivity, tomograph on the right side of Fig. 5 shows natural variations over the image block that are probably due to variations in soil type, soil compaction, moisture content, pore water salinity, etc. There is only a weak conductive anomaly associated with the UXO and it is not distinguishable from the larger natural variation in soil conductivity elsewhere in the image volume. The phase tomograph on the left side of Fig. 5, on the other hand, shows a 16 mrad negative anomaly close to the buried mass in an otherwise relatively uniform background of -6 to -8 mrad. The depth of the reconstructed anomaly is very close to what we expected although the lateral position was displaced 0.3 to 0.6 m. This error could be caused by smoothing from the inverse algorithm, from data errors, or from inaccuracies in marking of the UXO mass boundaries at the time of burial.

#### Controlled Test—3

The third controlled test was at the same site and was very similar to the second test. Again the 30 electrodes were arranged in a 5 by 6 rectangular pattern except that the spacing between adjacent electrodes was doubled to 1.8 m (6 feet) and the area covered was 7.3 by 9.1 m. Except for a scale factor, dictated by the new electrode spacing, the reconstruction mesh was identical with that used for the

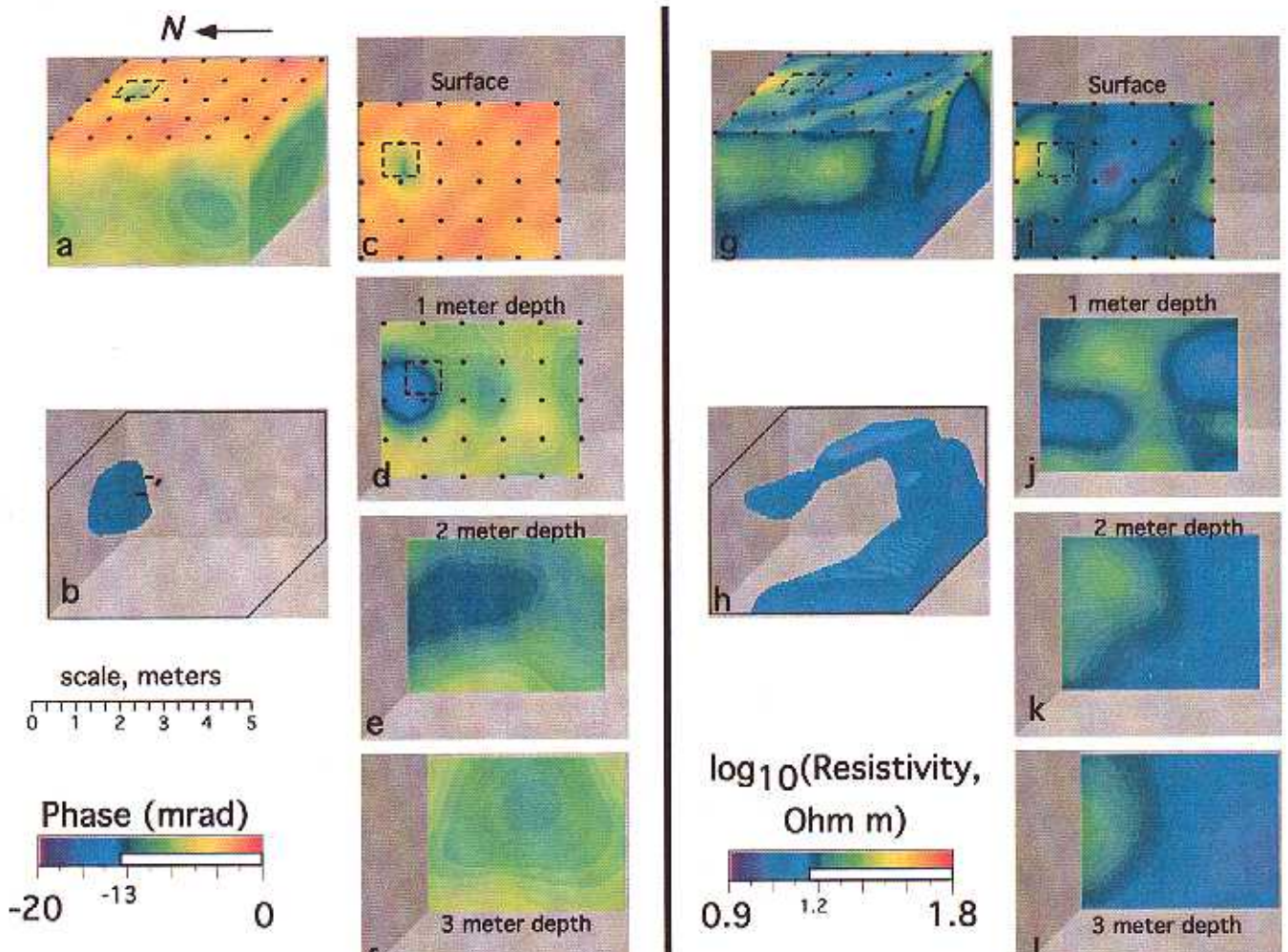


Figure 5. Three-dimensional impedance tomograph for controlled test 2 at Mare Island. Impedance phase (parts a through f) and impedance magnitude (parts g through l). UXO buried under the dashed square. There are two voxels between adjacent electrodes and the measurement frequency is 0.25 Hz. (a) Phase in milliradians (mrad) in the reconstruction block. (b) Reconstruction volume in part (a) is rendered transparent between 0 and  $-13$  mrad and the buried mass of UXO is imaged as a phase anomaly between  $-13$  and  $-20$  mrad. (c–f) Plan view sections of reconstruction block. (g) Impedance magnitude in Ohm-m in the reconstruction block. (h) Reconstruction volume is rendered transparent between 16 and 63 Ohm-m. (i through l) Plan view of depth sections in the reconstruction block.

second test. The purpose of this test was to determine the effects of the wider electrode spacing on sensitivity to the target. The results are shown in Fig. 6 using the same format of Fig. 5.

The tomographs in Fig. 6 are similar to those in Fig. 5 except for a reduced sensitivity to the target IP. This loss of sensitivity was expected because wider spacing means a reduced current density and correspondingly lower polarization at the soil-metal interface. Now we see an  $-8$  mrad phase anomaly at the target in a  $-6$  mrad background. This reconstruction also shows the natural phase response of the

soil increasing with depth. Although the mass can be seen right at the surface, at 1 m depth it is already lost in the background, and below 1 m other larger magnitude phase anomalies dominate. We conclude that the UXO is only marginally detected in this test due to the reduced sensitivity. Presumably, a larger amount of UXO would produce a larger phase anomaly and therefore would be more easily detected even at this larger electrode spacing.

From the three controlled tests described above we have evidence that electrode polarization at the metal soil boundary for typical UXO can be large enough to detect

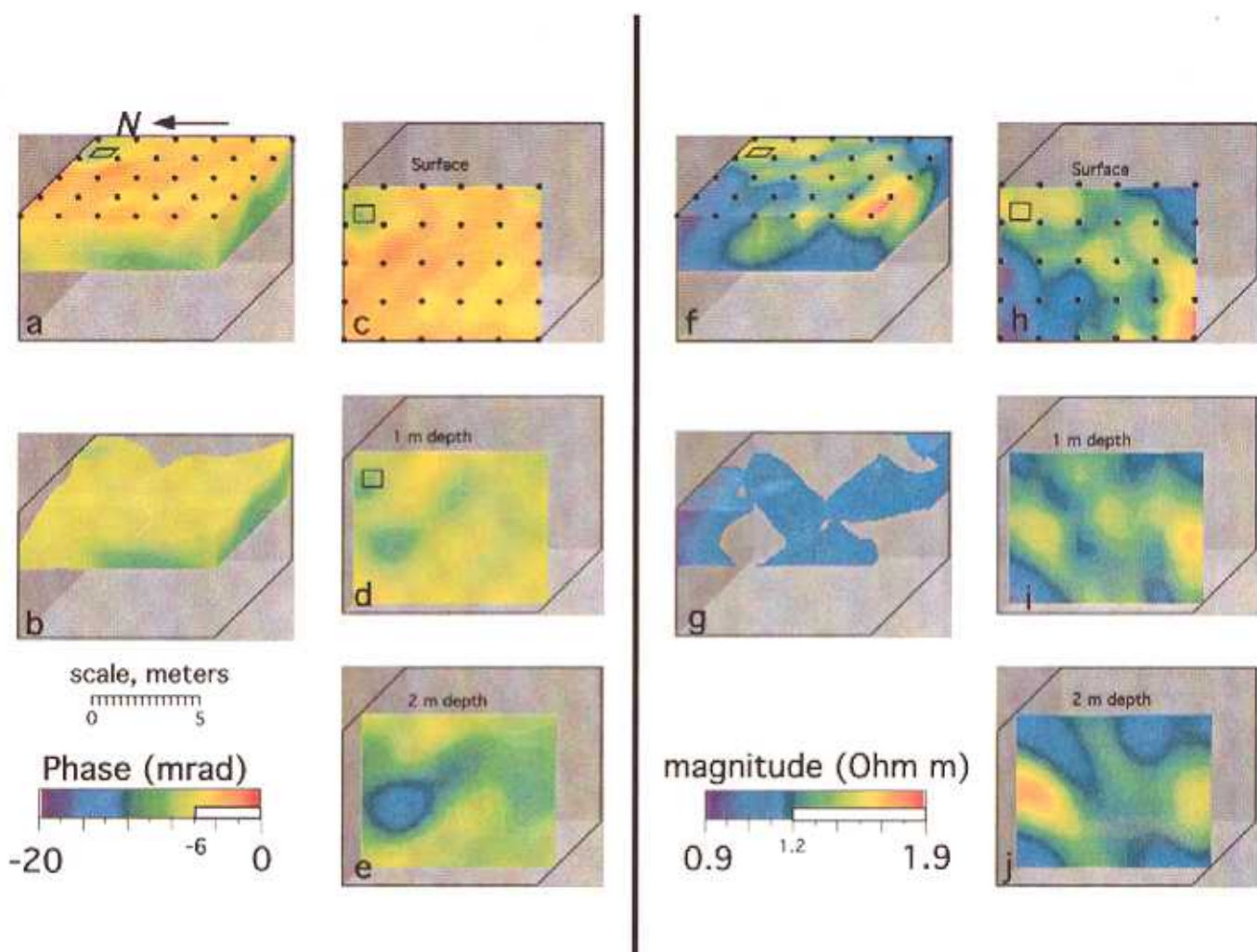


**Figure 6.** Three-dimensional impedance tomograph for controlled test 3 at Mare Island. Impedance phase (parts a through e) and impedance magnitude (parts f through j). UXO buried under the dashed square. There are three voxels between adjacent electrodes and the measurement frequency is 0.125 Hz. (a) Phase in milliradians (mrad) in the reconstruction block. (b) Reconstruction volume in part (a) is rendered transparent between 0 and  $-8$  mrad and the buried mass of UXO is imaged as a phase anomaly between  $-8$  and  $-20$  mrad. (c–e) Plan view sections of reconstruction block. (f) Impedance magnitude in Ohm-m in the reconstruction block. (g) Reconstruction volume is rendered transparent between 16 and 63 Ohm-m. (h through j) Plan view of depth sections in the reconstruction block.

and image using EIT. In fact, at two different sites, the reconstructed phase for a buried UXO mass was different enough from the background phase so as to be useful as a diagnostic for the target mass. Of course, the magnitude of phase anomaly is dependent, among other things, on the size of the mass as well as its proximity to the electrode array. All else being equal, a small mass will provide a smaller IP anomaly than a larger mass. Similarly, a mass that is further from the electrodes (*e.g.*, deeper) will have a smaller anomaly than if it is closer. It is this sensitivity to target size and location that prompted the third controlled test. It was the same as the second test but the larger electrode spacing put the mass farther from the electrodes with-

out changing other experiment parameters such as the mass size, pore water chemistry, or the IP response of the surrounding soil. The goal was to obtain information about the sensitivity limit for the method. We conclude from the second and third tests that for conditions found at this site, the UXO phase signal is significantly different from the background IP as long as the electrode spacing is less than 0.9 m. However, the UXO phase signal is of the same order as the background for electrode spacing of 1.8 m.

#### Blind Test – Site Description

A blind test was performed about 75 m from the second controlled test site, under a building (designated by the

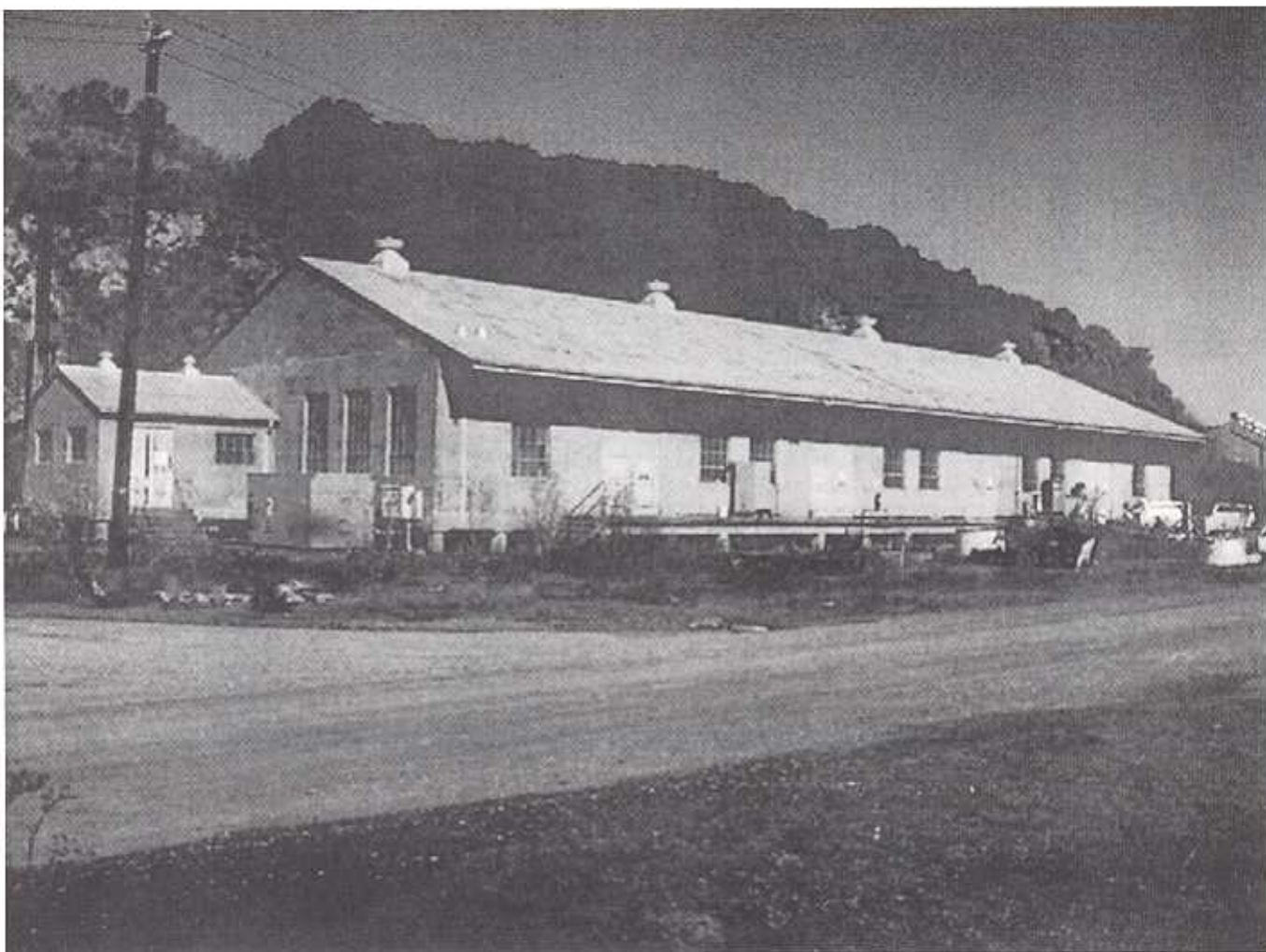


Figure 7. Building A259 at Mare Island, Ca.

Navy as A259) of the type formerly used at Mare Island for ordinance manufacture and handling. Figure 7 shows a picture of the building. Piles driven into the soil provide the functional support. The older buildings were set on wooden piles; in the more modern buildings, the footings and base were constructed of steel-reinforced concrete. The building base was laid, and the walls were constructed on the raised base. The roof was constructed to blow upward, permitting the force of an accidental explosion to be carried upward rather than outward through the walls. In many cases, the floor is raised, permitting access through a crawl-space. This is the typical construction for many buildings at Mare Island.

This site provided a convenient as well as a realistic location for a blind test. Mare Island began operations as an ordnance depot during the Civil War. In fact, about one half mile from A259, burial pits, each containing hundreds of Civil War era naval cannon projectiles, were excavated as part of the regular site remediation program. Building

A259 was built many years after the Civil War and therefore could well have been built over such a burial site. Prior to the test we had no knowledge of UXO beneath A259, making this location attractive for the blind test we wished to conduct.

The same electrode arrangement used at the last two controlled tests was used here, i.e., 30 electrodes, evenly spaced in a rectangular array. Electrodes were distributed under A259 so that each one was equidistant from all four adjacent piers, requiring an electrode spacing of 2.6 m. Figure 8 shows the arrangement. As we noted above, we expected that this wider spacing would impact sensitivity (*i.e.*, we would be looking for larger targets).

From this figure it is clear that there are many more than 30 electrode positions and yet the data acquisition system limited us to using 30 at a time. Therefore, the data were collected in 4 sets, each with 6 electrodes across the width of the building and 5 electrodes along the length. Each set of 30 overlapped the adjacent set by one row.

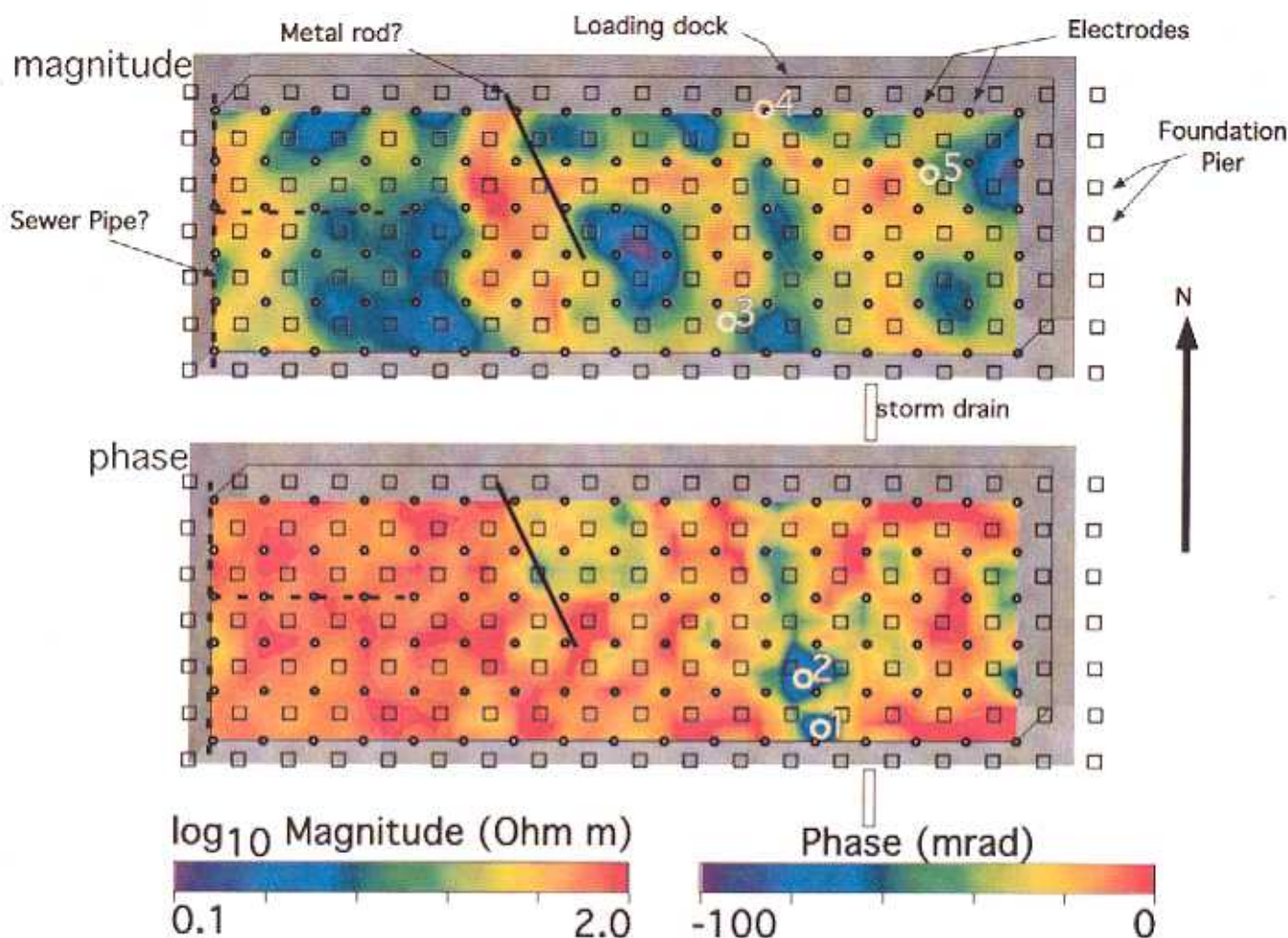


Figure 8. Impedance magnitude and phase tomographs for the blind test area under building A259 (see Fig. 7). Electrodes (dots) are evenly spaced between the foundation piers on an area 43 by 13.8 m and the impedance is reconstructed in a volume beneath the array. There are 3 voxels between adjacent electrodes and the measurement frequency is 0.25 Hz. Five locations selected for exploratory excavation are noted.

When combined, these 4 data sets produced a total of 102 electrode locations and 3,900 measurements for inversion. There were three reconstruction voxels (0.86 m on a side) between adjacent electrodes (2.6 m separation). The reconstruction volume is 41.3 m long, 12.9 m wide, and 6.9 m deep.

#### Blind Test Results

Data were taken and inverted for 0.25 Hz. Reconstruction of the impedance magnitude (resistivity) is shown in Fig. 8 but we will focus on the phase reconstruction as it is expected to reveal the most relevant diagnostic for UXO.

Two aspects of Fig. 8 are most apparent. First, the western part of the survey is relatively clear of phase anomalies when compared to the central and eastern parts. The only possible source of IP signal in the western end of the building is a shallow sewer pipe that apparently does not

contribute. Second, the phase anomalies are substantially larger in magnitude than those measured at the controlled test site. Phase values are reconstructed to almost  $-100$  mrad in a few locations whereas the largest shallow phase at the controlled site was about  $-20$  mrad. These values are larger than normally measured in soil and are difficult to explain by the presence of clay minerals alone (private communication, Slater).

The most significant phase anomalies under the western part of the building can be divided into three groups:

1. *An anomaly close to the metal rod which was lying on grade at the north side of the survey.* While it is tempting to attribute this feature to electrode polarization of the metal rod there are some reasons why this is a poor explanation. Most obvious is the fact that the rod is lying on the surface so that little surface area is in contact with soil. In addition, the reconstructed anomaly is not linear like the target.

2. A band of anomalies running north and south through the image volume in the vicinity of the storm drain on the south. These features constitute the bulk of the reconstructed anomalies and contain those largest in magnitude. Some of them persist with depth. These may be related to the presence of the storm drain at the southern edge of the building. Although this drain does not continue under the building, it may have affected the IP response of the soil nearby. We will discuss this hypothesis later.

3. A compact anomaly at the eastern edge of the image volume. This is a relatively small anomaly of low phase magnitude and has no clear source.

Although this test was blind, we were able to confirm the results after the test because limited digging was possible under the building. Five locations characterized by some of the negative phase anomalies were chosen for exploratory confirmation (locations are marked on Fig. 8). Using a truck-mounted vacuum system, a hole was dug at each location about 20 cm in diameter. The objective was to determine if metal, especially UXO, was buried at any of these locations.

The holes were excavated to the following depths: sites 1 and 2 to 1.2 m (4 ft), site 3 to 0.46 m (1.5 ft), site 4 to 1.8 m (6 ft) and site 5 to 1.5 m (5 ft). The material removed from the holes was searched for metal of any kind. Also, a metal detector was inserted into each hole to determine if metal was present nearby. This device is capable of sensing metal up to about 0.46 m away. Thus, the exploratory digging was limited to a very small volume relative to the size of each phase anomaly. During the excavation of the first three sites, three small metal objects were recovered.

- a) Galvanized pipe fitting:  $\frac{3}{4}$  inch, 45 degree elbow;
- b)  $\frac{1}{2}$  inch bolt about 1 inch long;
- c) spent .30 caliber brass casing.

The shell casing still bears the manufacturer's stamp indicating that it was manufactured in 1941. It is typical of the cartridges fired at one of the small arms ranges in operation at Mare Island at the time. Of course, these three objects, even taken together, are not sufficient to account for the -80 mrad anomaly at this location. Therefore, we conclude that the exploratory holes did not produce buried metal sufficient to explain the EIT phase anomalies.

## Discussion

Is there UXO beneath Building A259? The objective of the blind test was to evaluate the potential for EIT to answer this question under realistic conditions. The EIT survey delineated phase anomalies of sufficient magnitude and size to suggest buried UXO. While some metal objects were discovered, they are not, even taken together, suffi-

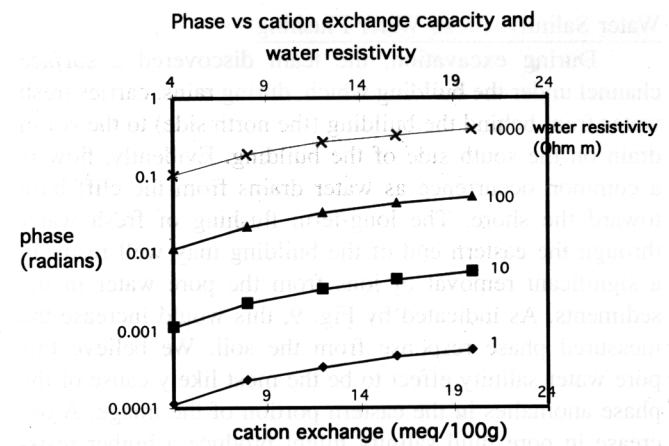


Figure 9. Effect of water resistivity and cation exchange capacity on phase (from Vinegar and Waxman, 1984).

cient to account for the anomalies present. The shell casing predates the construction of Building A259 by two years, which is sufficient to suggest that its burial predates the building as well. Therefore, it is possible that additional, but unconfirmed UXO is still under A259.

While some metal objects were found, other phenomena contributed to the phase signature as well. These include both the effects of differing lithology (and thus cation exchange capacity) and water salinity. Using Vinegar and Waxman's (1984) description, we have calculated the effect of changes in cation exchange capacity (CEC) and water salinity on phase. Figure 9 shows that increasing the fluid resistivity or CEC will increase the phase difference. Both of these effects appear to be at work in this case. Below we discuss how these effects influence the results of our blind test.

## Exotic Material: Changes in Cation Exchange Capacity (CEC)

During excavation, the team found the material beneath the western end of Building A259 to be more clay-rich, indicative of the sediments accreted along the southern edge of the island. The team also discovered that the material beneath the eastern end of the building is derived from the hillside behind the building. Part of the arkosic sandstone bedrock cliffs were knocked down prior to the building's construction, and the material was deposited over the area now covered by the eastern end of the building. Thus, the fill beneath the building varies from east to west, with the easternmost fill being capped by a more chaotic mix of former cliff material. The arkosic fill on the east might have a higher CEC and thus give rise to a more negative phase than the naturally-accreted sediments on the west. This might account for the higher phases imaged on the east end of A259.

### Water Salinity: Fresh Water Flushing

During excavation, the team discovered a surface channel under the building which, during rains, carries fresh water from behind the building (the north side) to the storm drain on the south side of the building. Evidently, flow is a common occurrence as water drains from the cliff base toward the shore. The long-term flushing of fresh water through the eastern end of the building may well result in a significant removal of ions from the pore water in the sediments. As indicated by Fig. 9, this would increase the measured phase response from the soil. We believe this pore water salinity effect to be the most likely cause of the phase anomalies in the eastern portion of the image. A decrease in pore fluid salinity might produce a higher resistivity in this area, however, the magnitude image does not show this. Therefore, this explanation is consistent with the resistivity image only if we realize that the resistivity is a function of other soil properties (*i.e.*, surface conduction) besides the pore fluid ion content.

### **Summary**

We have conducted surface EIT surveys over test sites in which various ordnance targets have been intentionally buried. In these controlled tests the targets consisted of a wide assortment of objects ranging from metal fuses to shell casings. Tomographs displaying magnitude alone sometimes show anomalies over the buried targets but also show other anomalies of equal or larger magnitude elsewhere in the survey area. However, in the phase tomographs, the strongest anomaly is centered over the buried target at two different test sites.

We found that the ability to discriminate between UXO IP and background or natural IP depends on electrode spacing. This fact is not a result of an intrinsic property of UXO but rather just a matter of sensitivity of the measurements and therefore, a function of the amount and distribution of the UXO, soil and pore water chemistry, measurement noise, etc., as well as electrode configuration. Under the conditions of our test, when electrode spacing was 0.9 m, the induced polarization from the metal appears larger than the naturally occurring background signal such that the UXO can be recognized as a distinct anomaly. However, when electrode spacing is doubled to 1.8 m, sensitivity to the same UXO signal is reduced so that the measured polarization from the metal is about the same as the background and the target can be identified only when its location is already known. Presumably, a larger UXO target with more total surface area would produce an anomaly of larger spatial size and phase shift and that would be more prominent in the phase reconstruction. Thus, detection limits are influenced by both the target mass size and proximity of the array to the target mass.

We also conducted a surface EIT survey over a test

site for which the content of buried UXO was unknown. This blind test was beneath a building that may have been built over an old UXO burial site. Tomographs of phase show shallow but strong phase anomalies of nearly -100 mrad under the eastern part of the building and relatively low phase elsewhere. These chargeabilities are larger than any seen at the other test sites and thus imply large concentrations of buried metal. Limited examination of the soil, however, yielded no concentrations of metal sufficient to cause these anomalies. The few pieces of scrap recovered suggest that at least some ordnance waste is present in the soil on which the building was built but the results of the limited sampling are inconclusive. Other effects contribute to the phase signal, including variations in lithology and the salinity of the pore fluid. Another blind test is planned, in which EIT will be deployed around and beneath a building under which is suspected UXO and which is slated for demolition. There, the EIT results can be verified by excavation.

### **Acknowledgments**

The authors wish to acknowledge the contributions of various individuals and organizations who provide valuable assistance and resources. D. LaBrecque and Xianjin Yang (Steamtech, Inc., Reno, Nev.) developed the 2D and 3D inverse algorithms used for this work. Clay Bodenhamer and Karl Hartman (Roy F. Weston, Vallejo, Calif.) generously provided assistance during field operations. Steve Hunter identified the provenance of the recovered casing. This project was administered by John Randall with funding provided by U.S. Navy Facilities Engineering Command, San Bruno, Calif.

*Work performed under the auspices of the U.S. Department of Energy by the Lawrence Livermore National Laboratory under Contract W-7405-Eng-48.*

### **References**

- Daily, W., and Owen, E., 1991, Cross-borehole resistivity tomography, *Geophysics*, **56**, 1228-1235.
- Dines, K.A., and Lytle, R.J., 1981, Analysis of electrical conductivity imaging, *Geophysics*, **46**, 1025-1036.
- Barber, D.C., and Seagar, A.D., 1987, Fast reconstruction of resistance images, *Clinical Physics and Physiological Measurement*, **8**, Suppl. A, 47-55.
- Frye, K.M., Lesmes, D.P., and Morgan, F.D., 1998, The influence of pore fluid chemistry on the induced polarization response of rocks and soils, *Proceedings of the Symposium on the Application of Geophysics to Engineering and Environmental Problems*, March 22-26, 1998, Chicago, Illinois, 771-780.
- Isaacson, D., 1986, Distinguishability of conductivities by electric current computed tomography, *IEEE Trans. on Medical Imaging*, vol. MI-5, no. 2, 91-95, June.
- Keevil, N.B., and Ward, S.H., 1962, Electrolyte activity: its effect on induced polarization, *Geophysics*, **27**, 677-690.

---

**Daily et al.: Imaging UXO using Electrical Impedance Tomography**

- Keller, G.V., and Frischknecht, F.C., 1966, Electrical methods in geophysical prospecting, Pergamon Press, Oxford.
- LaBrecque, D.J., Ramirez, A., Daily, W., Binley, A., and Schima, S., 1996, ERT Monitoring of Environmental Remediation Processes, *Meas. Sci. Technol.*, vol. 7, 375–383.
- Marshall, D.J., and Madden, T.R., 1959, Induced polarization, a study of its causes, *Geophysics*, 24, no. 4, 790–816.
- Oldenberg, D.W., and Li, Y., 1994, Inversion of induced polarization data, *Geophysics*, 59, 1327–1341.
- Pelton, W.H., Rijo, L., and Swift, Jr., C.M., 1978, Inversion of two-dimensional resistivity and induced-polarization data, *Geophysics*, 43, no. 4, 788–803, June.
- Ramirez, A., Daily, W., Binley, A., and LaBrecque, D., 1999, Electrical impedance tomography of known targets, *J. Env. Eng. Geoph.*, 4, 11–26.
- Sasaki, Y., 1992, Resolution of resistivity tomography inferred from numerical simulation, *Geophysical Prospecting*, 40, 453–463.
- Shi, W., Rodi, W., and Morgan, F.D., 1998, 3D induced polarization inversion using complex electrical resistivities: in Proc. of Symposium on the Application of Geophysics to Engineering and Environmental Problems, Chicago, Mar. 22–26, 1998, 785–794.
- SSPORTS Environmental Detachment, 1997, Unexploded ordnance site investigation of Mare Island Naval Shipyard, Vallejo, California, Final Summary Report, April 28.
- Telford, W.M., Geldart, L.P., Sheriff, R.E., and Keys, D.A., 1976, *Applied geophysics*, Cambridge Univ. Press, Cambridge.
- Tripp, A.C., Hohmann, G.W., and Swift, C.M., 1984, Two dimensional resistivity inversion, *Geophysics*, 49, 1708–1717.
- U.S. Army Environmental Center and the Naval Explosive Ordnance Disposal Technology Division, 1997, Report No. SFIM-AEC-CR-97011, UXO Technology Demonstration Program at Jefferson Proving Ground, Phase III, April.
- Van Voorhis, G.C., Nelson, P.H., and Drake, T.L., 1973, Complex resistivity spectra of porphyry copper mineralization, *Geophysics* 38, 49.
- Vinegar, H.J. and Waxman, M.H., 1984, Induced polarization of shaly sands, *Geophysics*, 49, 8, 1267–1287.
- Weller, A., Seichter, M., and Kampke, A., 1996, Induced polarization modelling using complex electrical conductivities, *Geophysical Journal International*, 127, 387–398.
- Wexler, A., Fry, B., and Neuman, M.R., 1985, Impedance-computed tomography algorithm and system, *Applied Optics*, 24, no. 23, 3985–3992, December.
- Yang, X., and LaBrecque, D., 1999, Comparison between stochastic and OCCAM's inversion of 3-D ERT data, SAGEEP 1999, Oakland, California, March, 979–988.
- Yorkey, T.J., Webster, J.G., and Tompkins, W.J., 1987, Comparing reconstruction algorithms for electrical impedance tomography, *IEEE Trans Biomedical Engineering*, BME-34, no. 11, 843–852, November.
- Yuval, and Oldenberg, D.W., 1997, Computation of Cole-Cole parameters using IP data, *Geophysics*, 62, no. 2, 436–448.